Comparative Analysis of two Types of Leg-observation-based Visual Servoing Approaches for the Control of a Five-bar Mechanism

Alessia Vignolo[1], **Sébastien Briot**[1], **Philippe Martinet**[1] and **Chao Chen**[2]
[1]IRCCyN, UMR CNRS 6597, École Centrale de Nantes, France
alessia.vignolo@gmail.com, {Sebastien.Briot, Philippe.Martinet}@irccyn.ec-nantes.fr
[2]Monash University, Clayton, Australia
chao.chen@monash.edu

Abstract

Past research works have proven that the robot end-effector pose of parallel mechanisms can be effectively estimated by vision. For parallel robots, it was previously proposed to directly observe the end-effector. However, this observation may be not possible (e.g. if the robot is milling). Therefore, it has been proposed to use another type of controller based on the observation of the leg directions. Despite interesting results, this controller involves the presence of mapping singularities inside the robot workspace (near which the accuracy is poor). This paper presents a new approach for vision-based control of the end-effector: by observing the mechanism legs, it is possible to extract the Plücker coordinates of their lines and control the end-effector pose. This paper shows also a comparison between the previous approach, based on the leg direction, and this new approach, based on the leg line Plücker coordinates. The new approach can be applied to a family of parallel machines for which the previous approach is not suitable and has also some advantages regarding the reachable workspace of the end effector. The simulation results of both the controllers applied on a five-bar mechanism are presented.

1 Introduction

Compared to serial robots, parallel kinematic manipulators [Leinonen, 1991] are stiffer and can reach higher speeds and accelerations [Merlet, 2006]. However, their control is troublesome because of the complex mechanical structure, highly coupled joint motions and many other factors (e.g. clearances, assembly errors, etc.) which degrade stability and accuracy.

Many research papers focus on the control of parallel mechanisms (see [Merlet, 2012] for a long list of references). It is possible to bypass the complex kinematic structure of the robot and to apply a form of control which uses an external sensor to estimate the pose of the end-effector, reducing the stability and accuracy degradation mentioned earlier.

A proven approach for estimating the end-effector pose is through the use of vision. The most common approach consists of the direct observation of the end-effector pose [Espiau *et al.*, 1992; Horaud *et al.*, 1998; Martinet *et al.*, 1996]. In some cases, however, it may prove difficult to observe the end-effector of the robot, e.g. in the case of a machine-tool. A substitute target for the observation must then be chosen and an effective candidate for this are the legs of the robot, which are usually designed with slim and rectilinear rods [Merlet, 2012].

An application of this technique was performed in [Andreff *et al.*, 2005] where vision was used to derive a visual servoing scheme based on the observation of the legs of a Gough-Stewart (GS) parallel robot [Gough and Whitehall, 1962]. In that method, the leg directions (each direction represented by a 3D unit vector) were chosen as visual primitives and control was derived based on their reconstruction from the image. The approach was applied to several types of robots, such as the Adept Quattro and other robots of the same family [Ozgur *et al.*, 2011; Andreff and Martinet, 2006].

However, it was proven later that:

- The mapping between the leg direction space and the end-effector pose space is not free of singularity which considerably affects the performance in terms of accuracy and which do not appear at the same place as the singularity of the controlled robot: finding the singularity of the mapping is a complicated task which can be considerably simplified by using a tool called "the hidden robot" concept [Rosenzveig *et al.*, 2014]. The hidden robot is a virtual robot whose kinematics represents the mapping between the leg direction space and the end-effector pose space. Thus, the mapping singularities appear if and only if the virtual hidden robot encoun-

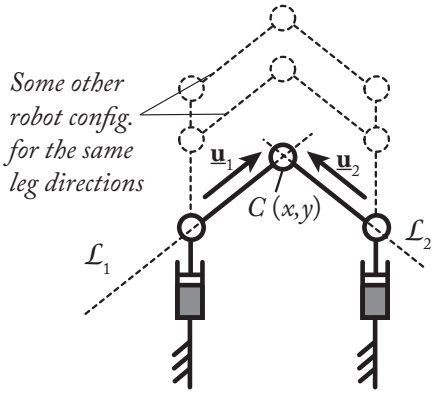

Figure 1: The $\underline{P}RRR\underline{P}$ robot

ters kinematic singularities. A general methodology to find the hidden robot model of any parallel robot controlled by leg-observation-based visual servoing approach has been defined in [Rosenzveig *et al.*, 2014] and several families of robots have been studied in [Briot and Martinet, 2013; Rosenzveig *et al.*, 2013; 2014].

- The approach proposed in [Andreff *et al.*, 2005] cannot be applied to any type of robot family: it was shown in [Andreff and Martinet, 2006] that it was not possible to control a particular family of parallel robots for which the first joints of the legs are prismatic joints whose directions are all parallel. For example, in the case of the $\underline{P}RRR\underline{P}$[1] robot with parallel $\underline{P}$ joints (Fig. 1), the pose of the end-effector can not be estimated using the leg directions $\underline{\mathbf{u}}_i$ as, for the same values of the vectors $\underline{\mathbf{u}}_1$ and $\underline{\mathbf{u}}_2$, infinite possible configurations of the end-effector can be found.

Regarding this second point, a solution to bypass the mentioned problem would be to use the Plücker coordinates of the lines passing through the legs instead of the leg directions only. Using the Plücker coordinates of the lines passing through the legs for the visual servoing is equivalent to use the leg direction plus their distance and position with respect to the camera frame. Thus, the line passing through the legs are fully defined. Estimating the end-effector pose in the case of the $\underline{P}RRR\underline{P}$ robot of Fig. 1 is similar to finding the intersection point of the lines $\mathcal{L}_1$ and $\mathcal{L}_2$ passing through the legs.

The aim of this paper is dual:

1. to introduce this new leg servoing scheme based on the use of the Plücker coordinates of the lines passing through the legs; to apply it on a five-bar mechanism; and to analyze the singularity of the mapping involved between the observed line space and the end-effector space, and
2. to compare this approach with the previous one based on the leg direction space in terms of robustness to measurement noise.

2 Leg observation

Both control schemes are based on the fact that it is possible to observe the robot legs. In this Section, the way to extract the leg direction and the Plücker coordinates of the line passing through the leg is discussed.

2.1 Line modeling

A line $\mathcal{L}$ in space, expressed in the camera frame, is defined by its Binormalized Plücker coordinates [Andreff *et al.*, 2002]:

$$\mathcal{L} \equiv ({}^c\underline{\mathbf{u}}, {}^c\underline{\mathbf{n}}, {}^cn) \tag{1}$$

where ${}^c\underline{\mathbf{u}}$ is the unit vector giving the spatial orientation of the line[2], ${}^c\underline{\mathbf{n}}$ is the unit vector perpendicular to the so-called interpretation plane of line $\mathcal{L}$ (which is the plane passing through the camera frame origin and the line $\mathcal{L}$) and ${}^cn$ is a nonnegative scalar. The latter are defined by ${}^cn{}^c\underline{\mathbf{n}} = {}^c\mathbf{P} \times {}^c\underline{\mathbf{u}}$ where ${}^c\mathbf{P}$ is the position of any point P on the line, expressed in the camera frame. Notice that, using this notation, the well-known (normalized) Plücker coordinates [Plücker, 1865; Merlet, 2006] are the couple $({}^c\underline{\mathbf{u}}, {}^cn{}^c\underline{\mathbf{n}})$.

The projection of such a line in the image plane, expressed in the camera frame, has for characteristic equation [Andreff *et al.*, 2002]:

$${}^c\underline{\mathbf{n}}^T{}^c\mathbf{p} = 0 \tag{2}$$

where ${}^c\mathbf{p}$ are the coordinates in the camera frame of a point P in the image plane, lying on the line.

With the matrix $\mathbf{K}$ formed by intrinsic parameters of the camera, one can obtain the line equation in pixel coordinates ${}^p\underline{\mathbf{n}}$ from:

$${}^p\underline{\mathbf{n}}^T{}^p\mathbf{p} = 0 \tag{3}$$

Indeed, replacing ${}^p\mathbf{p}$ with $\mathbf{K}{}^c\mathbf{p}$ in this expression yields:

$${}^p\underline{\mathbf{n}}^T\mathbf{K}{}^c\mathbf{p} = 0 \tag{4}$$

By identification of (2) and (3), one obtains

$${}^p\underline{\mathbf{n}} = \frac{\mathbf{K}^{-T}{}^c\underline{\mathbf{n}}}{\|\mathbf{K}^{-T}{}^c\underline{\mathbf{n}}\|}, {}^c\underline{\mathbf{n}} = \frac{\mathbf{K}^T{}^p\underline{\mathbf{n}}}{\|\mathbf{K}^T{}^p\underline{\mathbf{n}}\|} \tag{5}$$

[1] In the following of the paper, R and P stand for passive revolute and prismatic joints, respectively, while $\underline{R}$ and $\underline{P}$ stand for active revolute and prismatic joints, respectively.

[2] In the following of the paper, the superscript before the vector denotes the frame in which the vector is expressed ("b" for the base frame, "c" for the camera frame and "p" for the pixel frame). If there is no superscript, the vector can be written in any frame.

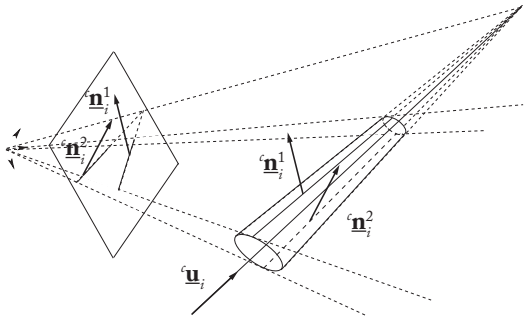

Figure 2: Projection of a cylinder in the image

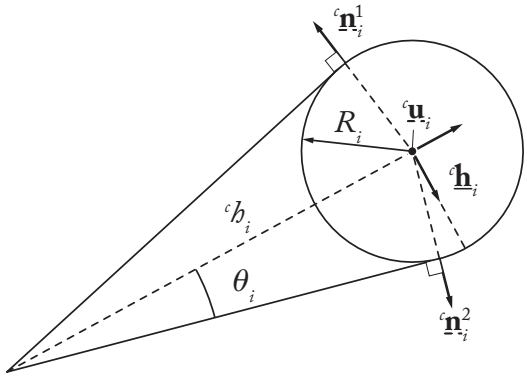

Figure 3: Visual edges of a cylinder

Notice that for numerical reasons, one should use normalized pixel coordinates. Namely, let us define the pixel frame by its origin located at the image center (i.e. the intersection of the image diagonals) and such that the pixel coordinates vary approximately between -1 and $+1$, according to the choice of the normalizing factor, which can be the image horizontal dimension in pixels, or its vertical dimension, or its diagonal.

2.2 Cylindrical leg observation

The legs of parallel robots have usually cylindrical cross-sections [Merlet, 2006]. The edges of the i-th cylindrical leg are given, in the camera frame, by [Andreff *et al.*, 2007] (Figs. 2 and 3):

$$^c\underline{\mathbf{n}}_i^1 = -\cos\theta_i\, ^c\underline{\mathbf{h}}_i - \sin\theta_i\, ^c\underline{\mathbf{u}}_i \times^c \underline{\mathbf{h}}_i \tag{6}$$

$$^c\underline{\mathbf{n}}_i^2 = +\cos\theta_i\, ^c\underline{\mathbf{h}}_i - \sin\theta_i\, ^c\underline{\mathbf{u}}_i \times^c \underline{\mathbf{h}}_i \tag{7}$$

where $\cos\theta_i = \sqrt{^ch_i^2 - R_i^2}\Big/{}^ch_i$, $\sin\theta_i = R_i/{}^ch_i$ and $(^c\underline{\mathbf{u}}_i, ^c\underline{\mathbf{h}}_i, ^ch_i)$ are the Binormalized Plücker coordinates of the cylinder axis and R_i is the cylinder radius.

It was also shown in [Andreff *et al.*, 2007] that the leg orientation, expressed in the camera frame, is given by

$$^c\underline{\mathbf{u}}_i = \frac{^c\underline{\mathbf{n}}_i^1 \times^c \underline{\mathbf{n}}_i^2}{\|^c\underline{\mathbf{n}}_i^1 \times^c \underline{\mathbf{n}}_i^2\|} \tag{8}$$

Let us remark now that each cylinder edge is a line in space, with Binormalized Plücker expressed in the camera frame $(^c\underline{\mathbf{u}}_i, ^c\underline{\mathbf{n}}_i^j, ^cn_i^j)$ (Fig 2). Moreover, any point A_i (of coordinates $^c\mathbf{A}_i$ in the camera frame) lying on the cylinder axis is at the distance R_i from the edge. Consequently, a cylinder edge is entirely defined by the following constraints, expressed here in the camera frame, although valid in any frame:

$$^c\underline{\mathbf{n}}_i^{jT}\, ^c\mathbf{A}_i = -R_i \tag{9}$$

$$^c\underline{\mathbf{n}}_i^{jT}\, ^c\underline{\mathbf{n}}_i^j = 1 \tag{10}$$

$$^c\underline{\mathbf{u}}_i^T\, ^c\underline{\mathbf{n}}_i^j = 0 \tag{11}$$

The vector $^c\mathbf{h}_i = {}^ch_i\, ^c\underline{\mathbf{h}}_i$ can be computed using the edges of the i-th cylindrical leg too, and it is given by

$$^c\mathbf{h}_i = {}^c\mathbf{D}_i \times {}^c\underline{\mathbf{u}}_i \tag{12}$$

where $^c\mathbf{D}_i$ is the position of the point B_i in the camera frame, which is the closest point of the axis of the i-th leg to the camera. It is given by

$$^c\mathbf{D}_i = \frac{R_i}{\sin(\theta_i)} \cdot \frac{^c\mathbf{n}_i^1 + {}^c\mathbf{n}_i^2}{\|^c\mathbf{n}_i^1 + {}^c\mathbf{n}_i^2\|} \tag{13}$$

3 Visual servoing schemes

In this Section, the control schemes for the visual servoing of a five-bar mechanism are defined and compared.

3.1 Kinematics of a five-bar mechanism

The planar five-bar mechanism (Fig. 4) is a 2 degrees-of-freedom (*dof*) parallel robot able to achieve two translations in the plane $(O, \mathbf{x}_0, \mathbf{y}_0)$ and which is composed of two legs:

- a leg composed of 3 R joints with an axis directed along $\mathbf{z}_0$ and located at points A_1, B_1 and C, the joint located at point A_1 being actuated, and
- a leg composed of 2 R joints with an axis directed along $\mathbf{z}_0$ and located at points A_2 and B_2, the joint located at point A_2 being actuated,

and other joints being passive. Thus, the vector of actuated coordinates is $\mathbf{q}^T = [q_1\ q_2]$. The end-effector is located at point C and its controlled coordinates along $\mathbf{x}_0$ and $\mathbf{y}_0$ are denoted as x and y, respectively.

The position of the point C is given by, for $i = 1, 2$:

$$\mathbf{C} = \mathbf{A}_i + l_{1i}\underline{\mathbf{v}}_i + l_{2i}\underline{\mathbf{u}}_i \tag{14}$$

where

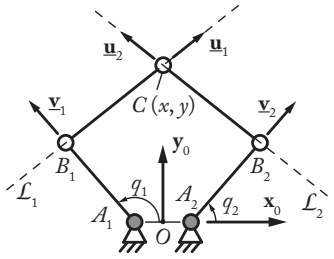

Figure 4: The planar five-bar mechanism (the gray pairs denote the actuated joints)

- $\mathbf{C}$ is the position of the point C, while $\mathbf{A}_i = [\delta_i\ 0]^T$ ($\delta_1 = -l_{OA_i}$ and $\delta_2 = +l_{OA_i}$) is the position of the point A_i (the frame is not specified, but it is usually either the base frame or the camera frame),
- l_{1i} and l_{2i} denote the length of the links A_iB_i and B_iC respectively,
- vectors $\underline{\mathbf{v}}_i$ and $\underline{\mathbf{u}}_i$ are unit vectors defining the direction of the links A_iB_i and B_iC respectively.

Rearranging (14), we obtain

$$\mathbf{C} - \mathbf{A}_i - l_{1i}\underline{\mathbf{v}}_i = l_{2i}\underline{\mathbf{u}}_i \tag{15}$$

Then, squarring both sides of (15) and suming the two lines, we get, for $i = 1, 2$:

$$(x - \delta_i - l_{1i}\cos q_i)^2 + (y - l_{1i}\sin q_i)^2 = l_{2i}^2 \tag{16}$$

Skipping all mathematical derivations, it comes that:

$$q_i = 2\tan^{-1}\left(\frac{-b_i \pm \sqrt{b_i^2 - c_i^2 + a_i^2}}{c_i - a_i}\right) \tag{17}$$

$a_i = -2l_{1i}(x-\delta_i)$, $b_i = -2l_{1i}y$, $c_i = (x-\delta_i)^2 + y^2 + l_{1i}^2 - l_{2i}^2$.

The first-order kinematics that relates the platform translational velocity $\boldsymbol{\tau}_p$ to the actuator velocities can be obtained through the differentiation of (16) with respect to time and can be expressed as:

$$\mathbf{A}\boldsymbol{\tau}_p + \mathbf{B}\dot{\mathbf{q}} = \mathbf{0} \tag{18}$$

where

$$\mathbf{A} = \begin{bmatrix} l_{21}\underline{\mathbf{u}}_1^T \\ l_{22}\underline{\mathbf{u}}_2^T \end{bmatrix} \tag{19}$$

$$\mathbf{B} = \begin{bmatrix} l_{11}l_{21}\underline{\mathbf{u}}_1^T\underline{\mathbf{v}}_1^\perp & 0 \\ 0 & l_{12}l_{22}\underline{\mathbf{u}}_2^T\underline{\mathbf{v}}_2^\perp \end{bmatrix} \tag{20}$$

with

$$\underline{\mathbf{v}}_i^\perp = \begin{bmatrix} -\sin q_i & \cos q_i \end{bmatrix}^T \tag{21}$$

Thus,

$$\boldsymbol{\tau}_p = -\mathbf{A}^{-1}\mathbf{B}\dot{\mathbf{q}} = \mathbf{J}\dot{\mathbf{q}} \tag{22}$$

or also

$$\dot{\mathbf{q}} = -\mathbf{B}^{-1}\mathbf{A}\boldsymbol{\tau}_p = \mathbf{J}_{pinv}\boldsymbol{\tau}_p \tag{23}$$

3.2 Leg-direction-based visual servoing of a five-bar mechanism

Kinematics of a five-bar mechanism using the leg-direction-based visual servoing technique

The control of a five-bar mechanism using the leg-direction-based visual servoing technique developed in [Andreff *et al.*, 2005] proposes to observe the leg direction $\underline{\mathbf{u}}_i$ to control the robot displacements. $\underline{\mathbf{u}}_i$ can be obtained directly from (15)

$$\underline{\mathbf{u}}_i = \left(\mathbf{C} - \mathbf{A}_i - l_{1i}\underline{\mathbf{v}}_i\right)/l_{2i} \tag{24}$$

Differentiating (24) with respect to time leads to:

$$\dot{\underline{\mathbf{u}}}_i = \left(\boldsymbol{\tau}_p - l_{1i}\underline{\mathbf{v}}_i^\perp\ \dot{q}_i\right)/l_{2i} \tag{25}$$

Finally, from (23), it comes that:

$$\dot{\underline{\mathbf{u}}}_i = \left(\mathbf{I}_3 + l_1\underline{\mathbf{v}}_i^\perp\mathbf{a}_i/b_{ii}\right)/l_{2i}\ \boldsymbol{\tau}_p = \mathbf{M}_{ui}^T\ \boldsymbol{\tau}_p \tag{26}$$

where $\mathbf{I}_3$ is the (3×3) identity matrix and matrix $\mathbf{M}_{ui}^T$ is called the interaction matrix.

It can be proven that matrix $\mathbf{M}_{ui}^T$ is of rank 1. As a result, a minimum of two independent legs is necessary to control the end-effector pose. An interaction matrix $\mathbf{M}_u^T$ can then be obtained by stacking the matrices $\mathbf{M}_{ui}^T$ of the two legs ($i = 1, 2$).

Control scheme and interaction matrix

Visual servoing is based on the so-called interaction matrix $\mathbf{M}^T$ [Chaumette, 2002] which relates the instantaneous relative motion $T_c = {}^c\tau_c - {}^c\tau_s$ between the camera and the scene, to the time derivative of the vector s, which is the vector staking all the visual primitives (which can be the legs directions or the legs Plücker coordinates) that are used through:

$$\dot{s} = \mathbf{M}_{(s)}^T T_c \tag{27}$$

where ${}^c\tau_c$ and ${}^c\tau_s$ are respectively the twists of the camera and the scene, both expressed in $\mathcal{R}_c$, i.e. the camera frame.

Then, one achieves exponential decay of an error $e(s, s_d)$ between the current primitive vector s and the desired one s_d using a proportional linearizing and decoupling control scheme of the form:

$$T_c = \lambda\hat{\mathbf{M}}_{(s)}^{T+}e(s, s_d) \tag{28}$$

where T_c is used as a pseudo-control variable and the upperscript + corresponds to the matrix pseudo-inverse.

The visual primitives being unit vectors, it is more elegant to use the geodesic error rather than the standard vector difference. Consequently, the error grounding the proposed control law will be:

$$\mathbf{e}_i = \underline{\mathbf{u}}_i \times \underline{\mathbf{u}}_{di} \tag{29}$$

where $\underline{\mathbf{u}}_{di}$ is the desired value of $\underline{\mathbf{u}}_i$.

Finally, a control is chosen such that E, the vector stacking the errors $\mathbf{e}_i$ associated to k legs ($k = 2...4$), decreases exponentially, i.e. such that

$$\dot{E} = -\lambda E \tag{30}$$

Then, introducing $\mathbf{N}_i^T = -[\underline{\mathbf{u}}_{di}]_\times \mathbf{M}_{ui}^T$ (where $[...]_\times$ is the antisymetric matrix associated to a 3D vector [Martinet *et al.*, 1996]), the combination of (26), (29) and (30) gives

$$\boldsymbol{\tau}_p = -\lambda \mathbf{N}^{T+} E \tag{31}$$

where $\mathbf{N}^T$ is obtained by stacking the matrices $\mathbf{N}_i^T$ of the two legs legs ($i = 1, 2$).

This expression can be transformed into the control joint velocities using (23):

$$\dot{\mathbf{q}} = -\lambda \mathbf{J}_{pinv} \mathbf{N}^{T+} E \tag{32}$$

3.3 Line-based visual servoing of a five-bar mechanism

In the present subsection, the controller based on the estimation of the Plücker coordinates of the lines passing through the legs is defined. This is the first time that such a controller is proposed.

Kinematics of a five-bar mechanism using the line-based visual servoing technique

The control of a five-bar mechanism using the new line-based visual servoing technique proposes to extract the Plücker coordinates $(\underline{\mathbf{u}}_i, \mathbf{h}_i)$ [3] of the two legs attached to the end-effector in order to control the robot displacements. The control can be done thanks to the fact that the point to control C is the intersection point of the lines of the two observed cylindrical legs. Applying the formula of the intersection point between two lines in a plane both expressed in Plücker coordinates, the position of the point C expressed in homogeneous coordinates is given by, for $i = 1, 2$ [Selig, 2005]:

$$\mathbf{C}_w = (-(\mathbf{h}_1 \cdot \mathbf{N}) \cdot \underline{\mathbf{u}}_2 + (\mathbf{h}_2 \cdot \mathbf{N}) \cdot \underline{\mathbf{u}}_1 + (\mathbf{h}_1 \cdot \underline{\mathbf{u}}_2) \cdot \mathbf{N} : (\underline{\mathbf{u}}_1 \times \underline{\mathbf{u}}_2) \cdot \mathbf{N}) \tag{33}$$

in which:

- $(\underline{\mathbf{u}}_1, \mathbf{h}_1)$ and $(\underline{\mathbf{u}}_2, \mathbf{h}_2)$ are the Plücker coordinates of the 1st and the 2nd leg respectively,
- $\mathbf{N}$ is a unit vector along a coordinate axis, with $(\underline{\mathbf{u}}_1 \times \underline{\mathbf{u}}_2) \cdot \mathbf{N}$ non-zero.

For converting the point from homogeneous to non-homogeneous coordinates, the first three coordinates of $\mathbf{C}_w$ have to be divided by the 4-th one. Moving the right term of (33) to the left side, extending it and naming the equations with f_i leads to

$$f_1 = x + h_{1z} u_{2x} - h_{2z} u_{1x} = 0 \tag{34}$$

$$f_2 = y + h_{1z} u_{2y} - h_{2z} u_{1y} = 0 \tag{35}$$

$$f_3 = z - h_{1x} u_{2x} - h_{1y} u_{2y} = 0 \tag{36}$$

$$f_4 = w - u_{1x} u_{2y} + u_{2x} u_{1y} = 0 \tag{37}$$

where (x, y, z, w) are the homogenous coordinates of $\mathbf{C}_w$; (u_{ix}, u_{iy}, u_{iz}) are the Cartesian components of the vector $\underline{\mathbf{u}}_i$; (h_{ix}, h_{iy}, h_{iz}) are the Cartesian components of the vector $\mathbf{h}_i$.

Differentiating (34), (35), (36) and (37) with respect to time leads to

$$\dot{x} - h_{2z}\dot{u}_{1x} + h_{1z}\dot{u}_{2x} + u_{2x}\dot{h}_{1z} - u_{1x}\dot{h}_{2z} = 0 \tag{38}$$

$$\dot{y} - h_{2z}\dot{u}_{1y} + h_{1z}\dot{u}_{2y} + u_{2y}\dot{h}_{1z} - u_{1y}\dot{h}_{2z} = 0 \tag{39}$$

$$\dot{z} - h_{1x}\dot{u}_{2x} - h_{1y}\dot{u}_{2y} - u_{2y}\dot{h}_{1x} - u_{2y}\dot{h}_{1y} = 0 \tag{40}$$

$$\dot{w} - u_{2y}\dot{u}_{1x} + u_{2x}\dot{u}_{1y} + u_{1y}\dot{u}_{2x} - u_{1x}\dot{u}_{2y} = 0 \tag{41}$$

Finally, putting (38), (39), (40) and (41) in matrix form, it comes that

$$\dot{\mathbf{l}} = -\mathbf{P}^+ \boldsymbol{\tau}_p = \mathbf{M}_l^T \boldsymbol{\tau}_p \tag{42}$$

where $\mathbf{l} = \begin{bmatrix} \underline{\mathbf{u}} \\ \mathbf{h} \end{bmatrix}$ and $p_{jk} = \frac{\partial f_j}{\partial l_k}$ is the term of the j-th row and the k-th column of $\mathbf{P}$, with $j = 1..4$ and $k = 1..12$.

Control scheme and interaction matrix

Because the vectors $\mathbf{h}_1$ and $\mathbf{h}_2$ are not unit vectors, the control law (27) cannot be used as it is. Consequently, it is necessary to use the following error

$$\mathbf{e}_i = \mathbf{l}_i - \mathbf{l}_{di} \tag{43}$$

where $\mathbf{l}_{di}$ is the desired value of $\mathbf{l}_i$.
The control is chosen in the same way of (30). From (30) and (43), it comes

$$-\lambda E = \dot{\mathbf{l}} - \dot{\mathbf{l}}_d \tag{44}$$

From (42) and (44), it is easy to derive the following control joint velocities

$$\dot{\mathbf{q}} = \mathbf{J}_{pinv} \cdot \mathbf{M}_l^{T+} \cdot (-\lambda E + \dot{\mathbf{l}}_d) \tag{45}$$

where $\mathbf{J}_{pinv}$ is the pseudo-inverse Jacobian matrix of the robot which relates the end-effector twist to the actuator velocities, i.e. $\mathbf{J}_{pinv} \boldsymbol{\tau}_p = \dot{\mathbf{q}}$.

4 Analysis of the controller singularities

In this Section, the control schemes for the visual servoing of a five-bar mechanism are compared in terms of singularities.

[3] In the paper, $\underline{\mathbf{h}}$ stands for unit vector, while $\mathbf{h}$ stands for non unit vector.

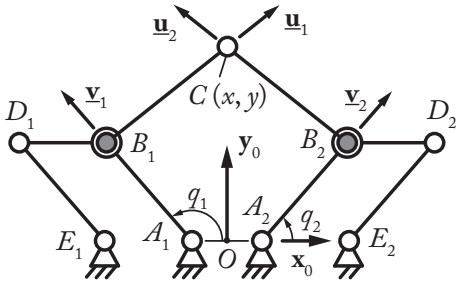

Figure 5: The hidden robot involved into the leg-direction-based visual servoing approach of a five-bar mechansim (the gray pairs denote the actuated joints)

4.1 Singularities of the controller using the leg-direction-based visual servoing technique

As mentioned in the introduction, the singularity of the mapping involved into the present controller can be analyzed through the aid of the "hidden robot" concept [Rosenzveig *et al.*, 2014]. The aim of this Section is not to present once again the "hidden robot" concept which has been shown in several papers [Rosenzveig *et al.*, 2014; Briot and Martinet, 2013; Rosenzveig *et al.*, 2013; 2014] but to directly use this tool to analyze the singularity of the controller. Therefore, we directly assert that the hidden robot involved into the leg-direction-based visual servoing approach for a five-bar mechansim is shown in Fig. 5. The reader willing to have further explanations is referred to [Rosenzveig *et al.*, 2014].

This virtual mechanism is made of two passive planar parallelogram joints $A_iB_iD_iE_i$ linked onto the ground on which is fixed an actuator at point B_i controlling the direction of the link B_iC. This special arrangement of the leg makes it possible, for one given position of the actuator at B_i, to maintain the orientation with respect to the base of the link B_iC independently of the configuration of the passive parallelogram joint.

A simple kinematic analysis of this virtual robot shows that:

- The Type 1 (or serial) singularities [Gosselin and Angeles, 1990] appear when one leg is fully stretched or folded, such as for a five-bar mechansim (Fig. 6),
- The Type 2 (or parallel) singularities [Gosselin and Angeles, 1990] appear when the links A_1B_1 and A_2B_2 are parallel, which is different from the Type 2 singularities of a five-bar mechanism that appear when the points B_1, B_2 and C are aligned (Fig. 7). As demonstrated in [Rosenzveig *et al.*, 2014], these singularities affect the performance of the controller in terms of accuracy and need to be well handled.

An example of singularity loci in the workspace of a given five-bar mechanism is provided in Fig. 8.

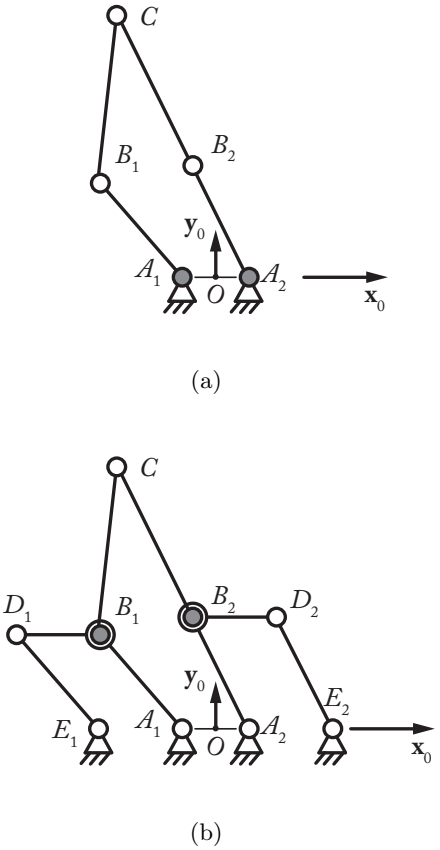

Figure 6: Examples of Type 1 singularity for a five-bar mechanism (a) and its corresponding hidden robot (b)

4.2 Singularities of the controller using the line-based visual servoing technique

It is known that the singularity conditions appear when the inverse or forward geometric model degenerates. The geometric models involved in this new controller are based on the fact that we can rebuild the end-effector pose by knowing the intersection point between the two lines $\mathcal{L}_1$ and $\mathcal{L}_2$ depicted in Fig 4. Therefore, the singularities appear when these two lines are parallel (intersection point at infinity) or coincide (infinity of possible intersection points). Such singularity conditions are equivalent to the Type 2 singularity conditions of a five-bar mechanism (Fig. 7(a)).

4.3 Discussion on the control schemes

At this step, it appears that the new controller has several advantages with respect to the approach proposed in [Andreff *et al.*, 2005] that should be clearly pointed out:

1. contrary to the past approach, as shown in Sections

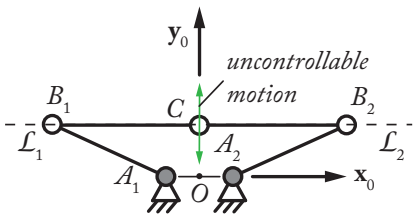

(a)

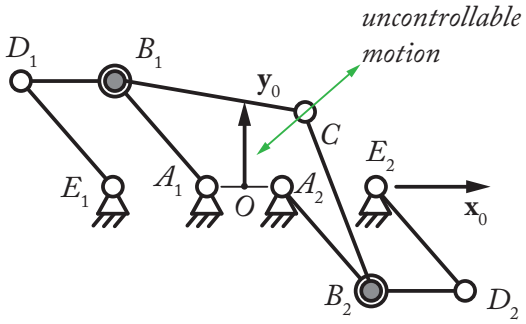

(b)

Figure 7: Examples of Type 2 singularity for a five-bar mechanism (a) and its corresponding hidden robot (b)

3.2 and 3.3, the new one does not need the use of the geometric parameters of the robot (except the radius of the observed cylinder) for estimating the platform pose. This is a great advantage because we only need to accurately calibrate the observed cylinders, not the entire robot, for obtaining the best robot accuracy,

2. the singularities of the new controller coincide with those of the real mechanism, which is a great advantage with respect to the past approach, for which the singularities are different and thus lead to the decrease of the reachable workspace.

In the next Section, the two control schemes are compared in terms of robustness to measurement noise in order to clearly demonstrate which type of controller is better.

5 Comparative analysis of the controller performance

In order to do a comparative analysis of the two control approaches, it has been created an Adams model of a five-bar mechanism with the following set of parameters: $l_{1i} = 0.3$ m as length of the legs attached to the ground, $l_{2i} = 0.35$ m as length of the legs attached to the end-effector, $l_{OA_i} = 0.275$ m as distance between O and A_i (Fig. 4). The workspace is plotted in Fig. 8. Both the leg-direction-based controller (case 1) and the line-based controller (case 2) have been applied to such a model.

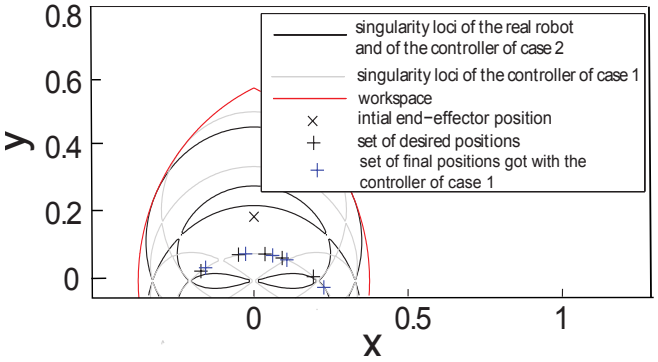

Figure 8: Singularity loci of a five-bar mechanism and its corresponding hidden robot for the following set of parameters: $l_{1i} = 0.3$ m, $l_{2i} = 0.35$ m, $l_{OA_i} = 0.275$ m.

5.1 Robustness to measurement noise near the singularity of the hidden robot of the controller based on the leg direction

We added noise on the measurements in order to compare the performance of both types of controller. First af all, the model that has been used for the visual servoing is a pinhole camera because it is simple to implement and is a good approximation of real cameras. In the Fig. 9 a camera with O as center of projection and the principal axis parallel to Z axis is shown. The distance between O and the image plane is the focal length f. The 3D point $P = (X, Y, Z)$ is projected on the image plane at coordinates $P_c = (u, v)$. The parameters of the camera used for the simulations are:
focal length with respect to $u = 10^3$ pixels;
focal length with respect to $v = 10^3$ pixels;
principle point in image along $u = 1024$ pixels;
principle point in image along $v = 768$ pixels.

The measurement noise is introduced like thereafter. The extraction of the Plücker coordinates of the leg line is based on the equations of the leg edges. In the simulation, they are projected to the image plane and converted from meter to pixel. Then, the edge line intersections with image boundary are computed: the coordinates of the intersection points have to be rounded due to the pixel accuracy. A new equation of

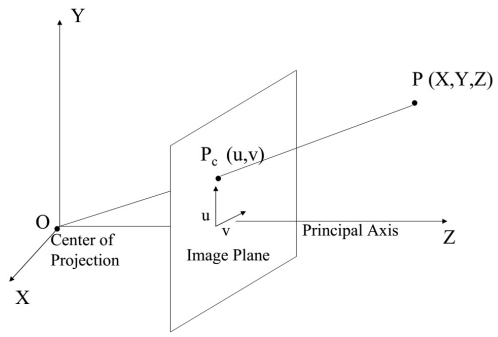

Figure 9: A pinhole camera model

the edge line is then recomputed taking into account the error introduced in the intersection points between the edge line and the image boundary.
In this subsection the results of the leg-direction-based and the line-based visual servoing approaches subjected to measurement noise are shown. The measurements error chosen is given by a pixel accuracy equal to 1. Then, it has been chosen the initial end-effector pose as $(x_0, y_0) = (0, 0.196)m$ and a set of desired positions $\mathbf{C}_d$ of the end-effector near the singularity of the hidden robot of the leg-direction-based controller:

- $\mathbf{C}_{d1} = (-0.172, 0.030)m$
- $\mathbf{C}_{d2} = (-0.050, 0.080)m$
- $\mathbf{C}_{d3} = (0.036, 0.082)m$
- $\mathbf{C}_{d4} = (0.092, 0.070)m$
- $\mathbf{C}_{d5} = (0.193, 0.013)m$

The initial position, the desired positions and the final positions got with the controller of case 2 are shown inside the plot of the workspace in Fig. 8 (from left to right, in black: $\mathbf{C}_{d1}...\mathbf{C}_{d5}$). The results of all the simulations are then shown in the Table 1: for each desired position, the final position and the error got with both the controller are shown. In the Table 1: $\mathbf{C}_d$ is the set of desired positions, $\mathbf{C}_{f1}$ and $\mathbf{C}_{f2}$ are the set of the final positions in the controllers of case 1 and case 2 respectively, $e_1(t_f)$ and $e_2(t_f)$ are the errors of the controllers of case 1 and case 2 respectively. The error is computed as the norm of the difference between the final position (the final time chosen is $t_f = 3s$) and the desired position. The graph on Fig. 10 shows the convergence of the end-effector pose of both controller in the case $\mathbf{C}_{d3} = (0.036, 0.082)m$.

Upon the results, it is readily found that the singularity of the hidden robot of the controller of case 2 is much more robust to measurement noise, which allows to access, with this new controller, the same workspace zones as the real robot (contrarily to the controller of case 1).

Table 1: Results of the simulations.

$\mathbf{C}_d$	$\mathbf{C}_{f1}$	$\mathbf{C}_{f2}$	$e_1(t_f)$	$e_2(t_f)$
(-0.172, 0.030)	(-0.157, 0.040)	(-0.173, 0.031)	0.0184	0.0013
(-0.05, 0.080)	(-0.027, 0.083)	(-0.050, 0.080)	0.0232	0.0004
(0.036, 0.082)	(0.061, 0.078)	(0.036, 0.083)	0.0255	0.0007
(0.092, 0.070)	(0.107, 0.065)	(0.092, 0.070)	0.0158	0.0003
(0.193, 0.013)	(0.227, -0.020)	(0.193, 0.013)	0.0471	0.0001

5.2 Crossing the hidden robot singularity

In this subsection, the end-effector desired position is chosen in such a way that the end-effector should cross the hidden robot singularity (singularity of the controller of case 1) shown in the Fig. 8. It is shown that in the case of leg-direction-based approach the legs direction converges to the desired one, but the end-effector position does not. While in the case of the line-based approach also the end-effector pose converges to the desired one. This is due to the fact that, in the controller of case 1, the five-bar mechanism converges to another assembly mode of its hidden robot.
The end-effector initial position is the same of the subsection (5.1), while the chosen desired position is $\mathbf{C}_d = (0.104, 0.036)m$. The results of the simulations are shown in Fig. 11.

6 Conclusions

In this paper, we proposed a new approach for vision-based control of the end-effector of a parallel robot. This method overcomes the disadvantages of the old vision-based controller based on the leg direction, proposed in the past papers, which are:

- it is not suitable for some PKM families (e.g. parallel robot whose legs directions are constant even if the end-effectors pose changes),
- it involves the presence of some models of robots, different from the real one, "hidden" into the controller (named "hidden robot model").

The new approach overcomes both the problems, and it is based on the Plücker coordinates of leg center line.

According to the simulations of both controllers on a five-bar mechanism, it was shown that the new approach is better because its hidden robot model has the same

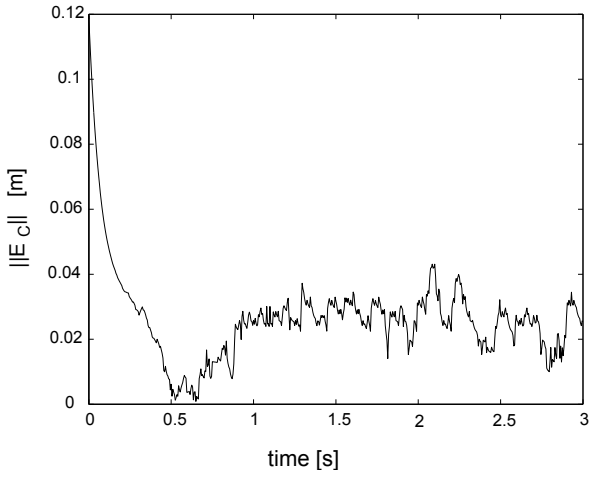

(a) End-effector pose error in the leg-direction-based controller.

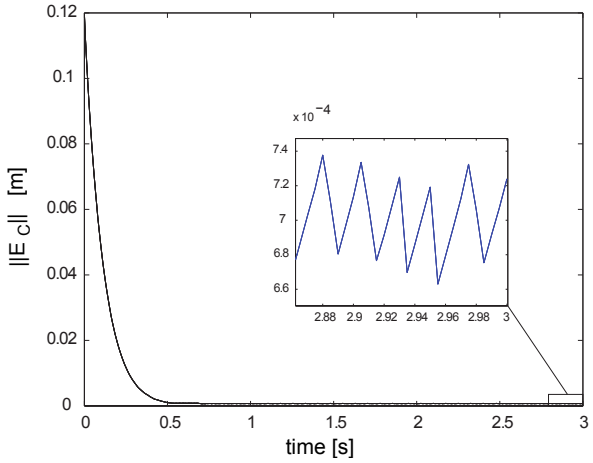

(b) End-effector pose error in the line-based controller.

Figure 10: Error in the case of measurement noise with desired position near the singularity of the leg-direction-based controller: $\mathbf{C}_{d3} = (0.036, 0.082)m$

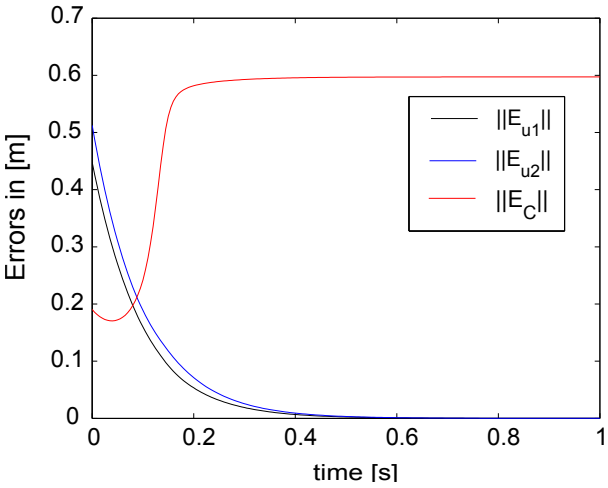

(a) Errors of the leg-direction-based controller.

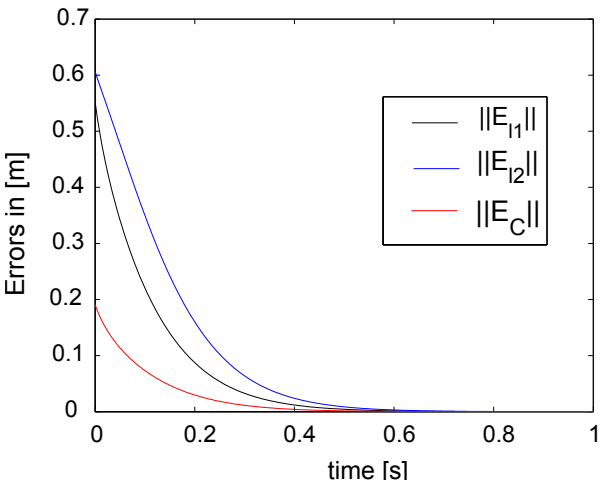

(b) Errors of the line-based controller.

Figure 11: Crossing the hidden robot singularity: $\mathbf{C}_d = (0.104, 0.036)m$

singularities as the real robot. Therefore, it is more robust to measure noise near the singularities of the hidden robot of the old approach and permits the mechanism to pass through singularities.
The new method is actually applicable for every parallel robot, both planar and spatial, indeed the five bar has been used just as an example here. Moreover, this method is not affected by the geometric parameters errors because it is completely independent from them.

References

[Andreff and Martinet, 2006] N. Andreff and P. Martinet. Vision-based kinematic modelling of some parallel manipulators for control purposes. In *Proceedings of EuCoMeS, the First European Conference on Mechanism Science*, Obergurgl, Austria, 2006.

[Andreff *et al.*, 2002] N. Andreff, B. Espiau, and R. Horaud. Visual servoing from lines. *International Journal of Robotics Research*, 21(8):679–700, 2002.

[Andreff *et al.*, 2005] N. Andreff, A. Marchadier, and P. Martinet. Vision-based control of a Gough-Stewart parallel mechanism using legs observation. In *Proceedings of the IEEE International Conference on Robotics and Automation, ICRA'05*, pages 2546–2551, Barcelona, Spain, April 18-22 2005.

[Andreff *et al.*, 2007] N. Andreff, T. Dallej, and P. Martinet. Image-based visual servoing of gough-stewart parallel manipulators using legs observation. *International Journal of Robotics Research*, 26(7):677–687, 2007.

[Briot and Martinet, 2013] S. Briot and P. Martinet. Minimal representation for the control of Gough-Stewart platforms via leg observation considering a hidden robot model. In *Proceedings of the 2013 IEEE International Conference on Robotics and Automation (ICRA 2013)*, Karlsruhe, Germany, May, 6-10 2013.

[Chaumette, 2002] F. Chaumette. *La commande des robots manipulateurs*. Hermès, 2002.

[Espiau *et al.*, 1992] B. Espiau, F. Chaumette, and P. Rives. A new approach to visual servoing in robotics. *IEEE Transactions on Robotics and Automation*, 8(3), 1992.

[Gosselin and Angeles, 1990] C.M. Gosselin and J. Angeles. Singularity analysis of closed-loop kinematic chains. *IEEE Transactions on Robotics and Automation*, 6(3):281–290, 1990.

[Gough and Whitehall, 1962] V.E. Gough and S.G. Whitehall. Universal tyre test machine. In *Proceedings of the FISITA 9th International Technical Congress*, pages 117–317, May 1962.

[Horaud *et al.*, 1998] R. Horaud, F. Dornaika, and B. Espiau. Visually guided object grasping. *IEEE Transactions on Robotics and Automation*, 14(4):525–532, 1998.

[Leinonen, 1991] T. Leinonen. Terminology for the theory of machines and mechanisms. *Mechanism and Machine Theory*, 26, 1991.

[Martinet *et al.*, 1996] P. Martinet, J. Gallice, and D. Khadraoui. Vision based control law using 3D visual features. In *Proceedings of the World Automation Congress, WAC96, Robotics and Manufacturing Systems*, volume 3, pages 497–502, Montpellier, France, May 1996.

[Merlet, 2006] J.P. Merlet. *Parallel Robots*. Springer, 2nd edition, 2006.

[Merlet, 2012] J.P. Merlet. www-sop.inria.fr/members/jean-pierre.merlet/merlet.html. 2012.

[Ozgur *et al.*, 2011] E. Ozgur, N. Andreff, and P. Martinet. Dynamic control of the quattro robot by the leg edgels. In *Proceedings of the IEEE International Conference on Robotics and Automation, ICRA11*, Shanghai, China, May 9-13 2011.

[Plücker, 1865] J. Plücker. On a new geometry of space. *Philosophical Transactions of the Royal Society of London*, 155:725–791, 1865.

[Rosenzveig *et al.*, 2013] V. Rosenzveig, S. Briot, and P. Martinet. Minimal representation for the control of the Adept Quattro with rigid platform via leg observation considering a hidden robot model. In *Proceedings of the IEEE/RSJ International Conference on Intelligent Robots and Systems (IROS 2013)*, Tokyo Big Sight, Japan, 2013.

[Rosenzveig *et al.*, 2014] V. Rosenzveig, S. Briot, P. Martinet, E. Ozgur, and N. Bouton. A method for simplifying the analysis of leg-based visual servoing of parallel robots. In *Proc. 2014 IEEE Int. Conf. on Robotics and Automation (ICRA 2014)*, Hong Kong, China, May 2014.

[Selig, 2005] J.M. Selig. Geometric fundamentals of robotics, 2005. Springer, 2nd edition.